

Do perfusion and diffusion MRI predict glioblastoma relapse sites following chemoradiation?

Jonathan Khalifa^{1,2} · Fatima Tensaouti¹ · Jean-Albert Lotterie^{1,3} · Isabelle Catalaa^{1,4} · Leonor Chaltiel⁵ · Alexandra Benouaich-Amiel⁶ · Carlos Gomez-Roca⁷ · Georges Noël⁸ · Gilles Truc⁹ · Patrice Péran^{1,10} · Isabelle Berry^{1,3,10} · Marie-Pierre Sunyach¹¹ · Marie Charissoux¹² · Corinne Johnson¹³ · Elizabeth Cohen-Jonathan Moyal^{2,14,15} · Anne Laprie^{1,2,14}

Received: 15 January 2016 / Accepted: 31 July 2016 / Published online: 8 August 2016
© Springer Science+Business Media New York 2016

Abstract To assess the value of T2* dynamic-susceptibility contrast MRI (DSC-MRI) and diffusion-weighted imaging (DWI) to predict the glioblastoma relapse sites after chemoradiation. From a cohort of 44 patients, primarily treated with radiotherapy (60 Gy) and concomitant temozolomide for glioblastoma, who were included in the reference arm of a prospective clinical trial (NCT01507506), 15 patients relapsed and their imaging data were analyzed. All patients underwent anatomical MRI, DSC-MRI and DWI before radiotherapy and every 2 months thereafter until relapse. Voxels within the sites of relapse were correlated with their perfusion and/or diffusion abnormality

(PDA) pretreatment status after rigid co-registration. The relative cerebral blood volume (rCBV) and apparent diffusion coefficient (ADC) were used as biomarkers. Several PDA areas were thresholded: hyperperfused voxels using a 1.75 fixed rCBV threshold (HP_f); hypoperfused (hP_g) and hyperperfused (HP_g) voxels using a histogram-based Gaussian method; diffusion-restricted voxels (DR_g); and HP_g voxels with diffusion restriction (HP_g&DR_g). Two sets of voxels (2,459,483 and 2,073,880) were analyzed according to these thresholding methods. Positive predictive values (PPV) of PDA voxels were low (between 9.5 and 31.9%). The best PPV was obtained with HP_g&DR_g

✉ Jonathan Khalifa
jonathan.khalifa@hotmail.fr

¹ INSERM UMR 1214, TONIC (Toulouse NeuroImaging Centre), 31059 Toulouse, France

² Department of Radiation Oncology, Institut Claudius Regaud/Institut Universitaire du Cancer de Toulouse-Oncopole, 1 avenue Irène-Joliot Curie, 31100 Toulouse, France

³ Department of Nuclear Medicine, CHU Rangueil, 1 Avenue du Professeur Jean Poulhès, 31400 Toulouse, France

⁴ Department of Radiology, CHU Rangueil, 1 Avenue du Professeur Jean Poulhès, 31400 Toulouse, France

⁵ Department of Biostatistics, Institut Claudius Regaud/Institut Universitaire du Cancer de Toulouse-Oncopole, 1 avenue Irène-Joliot Curie, 31100 Toulouse, France

⁶ Department of Medical Oncology, Institut Claudius Regaud/Institut Universitaire du Cancer de Toulouse-Oncopole, 1 avenue Irène-Joliot Curie, 31100 Toulouse, France

⁷ Clinical Research Unit, Institut Claudius Regaud/Institut Universitaire du Cancer de Toulouse-Oncopole, 1 avenue Irène-Joliot Curie, 31100 Toulouse, France

⁸ Department of Radiation Oncology, Centre Paul Strauss, EA 3430, University of Strasbourg, 3 rue de la Porte de l'Hôpital, 67065 Strasbourg, France

⁹ Department of Radiation Oncology, Centre Georges-François Leclerc, 1 rue Professeur Marion, 21079 Dijon, France

¹⁰ Université Toulouse III Paul Sabatier, UMR 1214, 31059 Toulouse, France

¹¹ Department of Radiation Oncology, Centre Léon Bérard, 28 Rue Laënnec, 69373 Lyon, France

¹² Department of Radiation Oncology, Institut du Cancer de Montpellier, 208 avenue des Apothicaires, parc Euromédecine, 34298 Montpellier cedex 5, France

¹³ Christie Medical Physics and Engineering, The Christie NHS Foundation Trust, Manchester M20 4BX, UK

¹⁴ Université Toulouse III Paul Sabatier, 31000 Toulouse, France

¹⁵ INSERM U1037, Centre de Recherches contre le Cancer de Toulouse, 1 avenue Irène-Joliot Curie, 31100 Toulouse, France

voxels within the FLAIR hyperintensity, as 18.3 % of voxels without initial PDA were within relapse sites, versus 31.9 % with initial PDA ($p < 0.0001$). This prospective study suggests that DSC and/or DWI-MRI do not predict the glioblastoma relapse sites. However, further investigations with new methodological approaches are needed to better understand the role of these modalities in the prediction of glioblastoma relapse sites.

Keywords Perfusion weighted magnetic resonance imaging · Diffusion weighted magnetic resonance imaging · Glioblastoma · Sites of relapse · Voxel-based quantification

Introduction

Glioblastoma multiforme (GBM) is the most common primary brain tumor in adults. Despite major advances in the management of GBM over the past decade, the outcome of patients still remains poor [1]. Most relapses occur within 2 cm of the contrast enhancement, and almost exclusively in the edema area [2–4]. Efforts are therefore needed to improve the GBM local control after chemoradiation.

GBM is an infiltrating and heterogeneous brain tumor characterized by high cellular proliferation, high cellular density and active angiogenesis associated with areas of necrosis. Therefore, one promising strategy to improve local control consists of heterogeneously irradiating the target volume, with focal increases in dose targeted at radioresistant clusters defined by metabolic imaging [5]. This *dose-painting* approach should target metabolic abnormalities that are not only prognostic indicators of aggressiveness, but also predictive of local relapse after treatment.

Several data are available with ^1H magnetic resonance spectroscopic imaging, using either the choline/*N*-acetyl-aspartate (NAA) ratio (reflecting high membrane turnover), or the lactate/NAA ratio (as a surrogate of hypoxia), as predictive markers of relapse sites [6–9]. As a further step, several prospective studies are currently being conducted to assess the benefit of a dose escalation specifically on spectral abnormalities, while the whole classical treatment volume is receiving the standard dose of treatment.

The two other functional MR imaging techniques commonly used for gliomas are perfusion MRI (mainly T2*-weighted dynamic-susceptibility contrast MRI (DSC-MRI) or dynamic contrast-enhanced MRI (DCE-MRI)) and diffusion MRI (diffusion-weighted imaging (DWI)). The relative Cerebral Blood Volume (rCBV) which is derived from DSC-MRI is a surrogate for tumor perfusion. The apparent diffusion coefficient (ADC) is derived from DWI and indirectly reflects cell density through the evaluation of the apparent diffusivity of water molecules. Many data are available on the prognostic value of rCBV and

ADC in GBM [10–13], and these techniques could be complementary [14, 15]. However, very few data are available on their predictive value for the sites of relapse after treatment [16].

The objective of this study was thus to prospectively assess the value of pre-radiotherapy rCBV and ADC (alone or combined) as biomarkers of the sites of GBM relapse after standard treatment, to better understand how we should integrate DSC-MRI and DWI within the treatment planning step to guide potential focal increases in dose within the standard treatment volume.

Materials and methods

Patients

Forty-four patients with pathologically proven GBM, who were enrolled in the reference arm of a phase-III randomized multicentre prospective clinical trial (NCT01507506), were primarily treated with radiotherapy (60 Gy) and concomitant temozolomide [1]. Main inclusion criteria were: age > 18 years-old, WHO performance status ≤ 2 , and unifocal GBM with either resectable or unresectable disease, but largest tumor diameter ≤ 5 cm. Among them, 15 patients who were included from March 2011 to December 2013, and who were found to have relapsed at the cut-off date of February 2015, were analyzed in this ancillary study. Their median age was 63.5 years (range: 35–83). MGMT promoter was methylated in five patients, and unmethylated in ten patients. All patients received radiotherapy after surgical resection (gross total resection/near gross total resection (GTR) for eight patients and subtotal resection (STR) for seven patients). All patients provided written informed consent. The protocol was approved by the national French ethics committee (*Comité de Protection des Personnes*, approval number: 2009-A00594-53). Insurance was underwritten for each patient in accordance with French biomedical legislation.

Chemoradiotherapy

Radiotherapy was delivered once a day, five times a week, over a 6-week period, in fractions of 2 Gy to give a total dose of 60 Gy, using either intensity modulated radiotherapy or 3D conformal radiotherapy. The Gross Tumor Volume (GTV) was defined as the contrast-enhanced lesion on T1-weighted MRI or the surgical cavity with residual contrast-enhancement. The Clinical Target Volume (CTV) was built with a 17-mm isotropic margin around the GTV and was required to encompass all the FLAIR abnormalities [1]. Finally, the Planning Target Volume (PTV) was built with a 3-mm isotropic margin expansion around the CTV. The concomitant and adjuvant chemotherapy with temozolomide was delivered according to the standard of care [1].

Table 1 Number of days between surgery and pre-radiotherapy baseline imaging, and between surgery and every follow-up (FU) examination until recurrence

Pt	Baseline imaging	FU1	FU2	FU3	FU4	FU5	FU6	FU7
1	21*, §	168	226	–	–	–	–	–
2	22	162	219*	273	332	–	–	–
3	27§	167	223*	286	–	–	–	–
4	22*, §	163§	210§	260§	–	–	–	–
5	27	162	220	276*	331	388	443	499
6	23§	158	215	270*	331	384	–	–
7	27§	163§	215§	275*, §	345§	400§	464	515
8	21*	156§	–	–	–	–	–	–
9	26*	170§	–	–	–	–	–	–
10	23§	163*, §	219§	288§	349§	–	–	–
11	27*, §	164§	224§	–	–	–	–	–
12	20	164	228	270*	332	389	–	–
13	22	166*	226	–	–	–	–	–
14	27*	169	–	–	–	–	–	–
15	27*	150	–	–	–	–	–	–

*MR scan used as a reference to delineate the site of relapse (baseline imaging or nadir examination in case of tumor shrinkage within the follow-up)

§Patient on corticosteroid at the time of the MR scan

MR data acquisition

All scans from each of the centres included in the trial were performed on a Siemens 1.5-T MRI scanner (Siemens, Erlangen, Germany) with a standard 12-channel head coil. Parallel imaging acquisition method was used for each patient, based on the GRAPPA (Generalized autocalibrating partially parallel acquisition) reconstruction algorithm, with an acceleration factor of 2. The anatomical MRI protocol included: acquisition of 3 mm-thick axial images [turbo spin-echo T2-weighted imaging (TR/TE=4200/97 ms), fluid-attenuated inversion recovery imaging (FLAIR: TR/TI/TE=6500/2400/121 ms)] with a field of view (FOV) of 172×230 mm² and a matrix size of 256×192, resulting in a voxel size of 0.9×0.9×3 mm³; and acquisition of 1 mm-thick 3D T1-weighted images (T1) before and after injection of a standard dose of 15 ml of gadolinium-based contrast agent (Gadobenate dimeglumine, MultiHance®) (T1-Gd: TR/TE=11/5.2 ms, FOV=256×224 mm², matrix size=256×224, resulting in a voxel size of 1×1×1 mm³).

For DSC-MRI, a series of 34 volumes of 39 slices were acquired at 1.09-second intervals, with a gradient-echo echo-planar imaging sequence (TR/TE=4720/47 ms, FOV=230×230 mm², matrix size=128×128, flip angle=90°), during the first pass of a standard dose (0.1 mmol/kg) bolus of gadolinium. Gadolinium was injected intravenously using a power injector at a rate of 5 mL/s, immediately followed by a saline injection.

DWI was performed with a single-shot, spin-echo, echo-planar imaging sequence in the axial plane (TR/TE=8300/91 ms at b=0 and b=1000 s/mm², 25–40 sections, 2-mm section thickness, FOV=230×230 mm², matrix size=192×192). DWI was acquired in three orthogonal directions.

Anatomical and perfusion/diffusion MR imaging was performed one week before RT, 3 months after the end of radiotherapy, and every following 2 months until relapse (Table 1). The pre-RT images were used as the baseline assessment. All the cases enrolled in this study were discussed at the local neuro-oncological Multi-Disciplinary Team meeting of each centre, to validate or not the progression. Progression was defined according to the Response Assessment in Neuro-Oncology Working Group (RANO) criteria [17] and every relapse was centrally reviewed by an experienced neuroradiologist (I.C.). During follow-up, if there was uncertainty regarding progression or pseudo-progression, a subsequent evaluation was performed 4 weeks later. If subsequent evaluations suggested that the patient was experiencing progression, then the date of progression was defined as the time point at which this issue was first raised.

Image registration

All image data were rigidly co-registered to the pre-treatment 3D T1-Gd images using mutual information as a similarity measure and Nelder–Mead simplex method as an optimization regime [18]. Every automatic co-registration was visually verified and validated using a combination of methods, including split-screen, scrolling slice by slice in different planes, as well as comparing contour overlays.

Data processing

The Figs. 1 and 2 illustrate the data processing and spatial analysis steps for two representative cases: one STR patient (Fig. 1) and one GTR patient (Fig. 2).

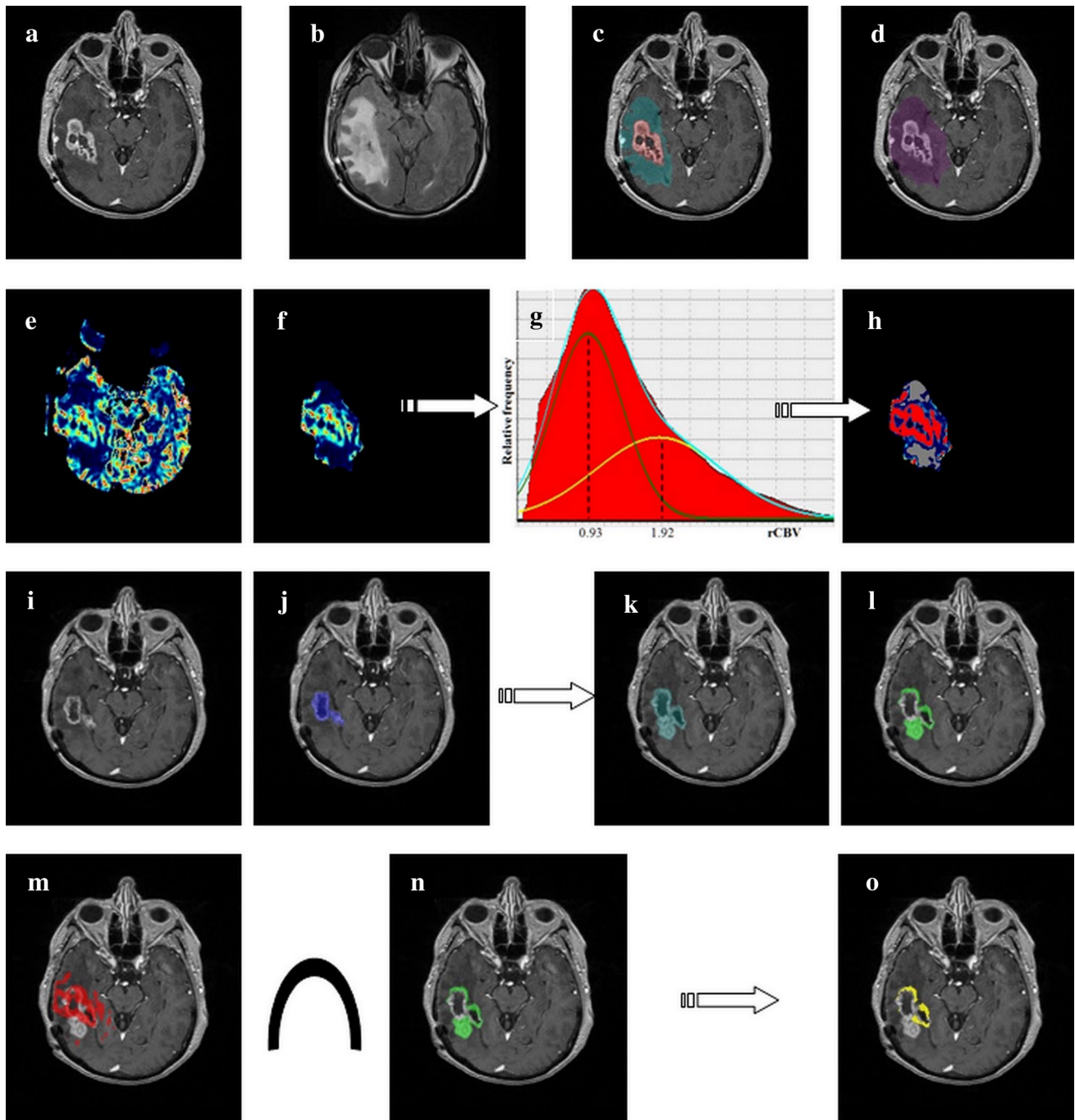


Fig. 1 Example of data post-processing to obtain true positive hyperperfused voxels with the Gaussian method (HP_g) within the target volume for a representative case of sub-total resection. Pre-radiotherapy T1-weighted images with gadolinium (**a**) and FLAIR images (**b**) were delineated to obtain the hyperFLAIR volume (cyan) (**c**) and the target volume (purple) (**d**). A relative cerebral blood volume (rCBV) map was obtained with Olea[®] software (**e**), and rCBV values (>0.2) were thresholded within the target volume (**f**). The Gaussian thresholding method (**g**) consisted of a bi-Gaussian fitting of the rCBV histogram. Hypoperfusion and hyperperfusion thresholds corresponded to the mean of the lower Gaussian curve (0.93 for this patient) and the mean of the upper Gaussian curve (1.92), respectively. By applying these

thresholds within the target volume, we could then identify: hypoperfused voxels (hP_g , dark gray) and hyperperfused voxels (HP_g , red) (**h**). The site of relapse (light green) (**l**) was defined as the contrast enhancement plus necrotic regions at relapse (dark green) (**k**), excluding contrast-enhancement plus necrotic regions at nadir examination (blue) (**i**, **j**) (case of tumor shrinkage after chemoradiation). Finally, the true positive voxels (yellow) were the site of relapse voxels within initial HP_g (**m**, **n**, **o**). In the case of HP_g within hyperFLAIR, the true positive voxels were the site of relapse voxels within initial HP_g and hyperFLAIR volume. All images were co-registered with pre-radiotherapy T1-Gd MRI

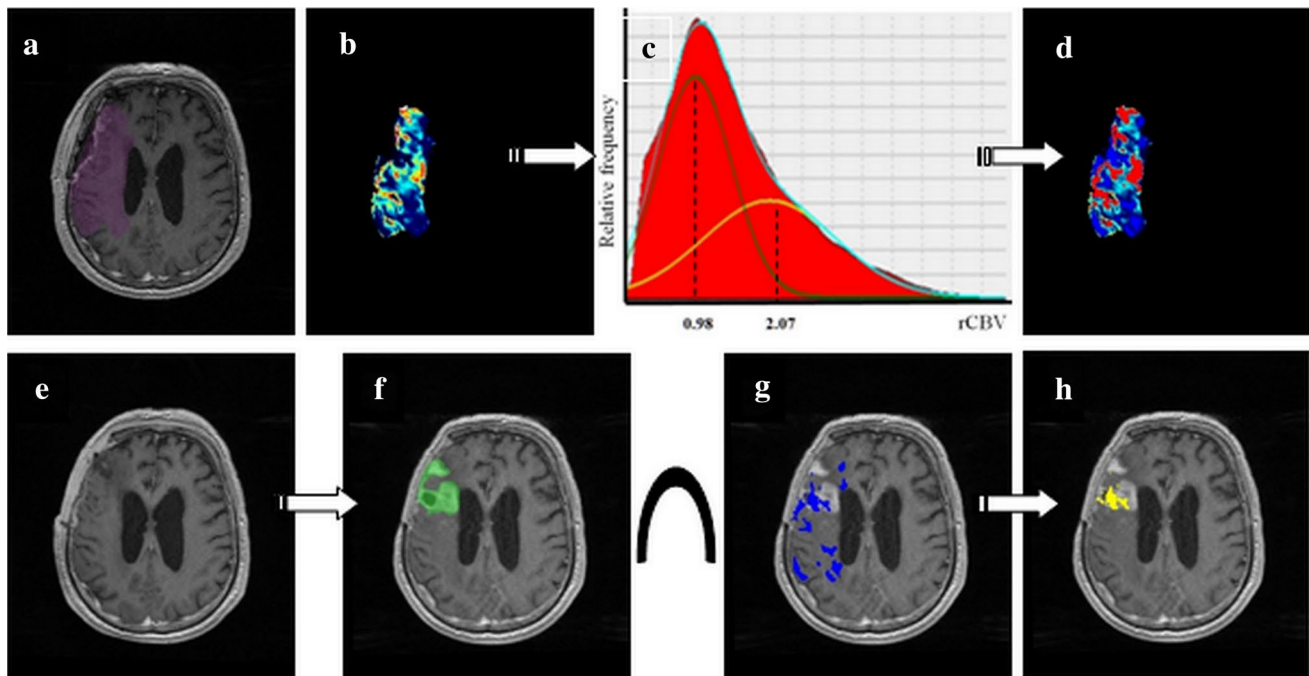


Fig. 2 Similar example of data post-processing to obtain true positive hypoperfused voxels with the Gaussian method (hP_g) within the target volume for a representative case of gross-total resection. The target volume (TV) was obtained after delineation of the surgical cavity with a 17-mm isotropic margin and with inclusion of all the FLAIR abnormalities: this TV is displayed in purple on the pre-radiotherapy T1-weighted images with gadolinium (a). The relative cerebral blood volume (rCBV) map was thresholded within the target volume (b). The Gaussian thresholding method (c) consisted of a bi-Gaussian fitting of the rCBV histogram. Hypoperfusion and hyperperfusion thresholds

corresponded to the mean of the lower Gaussian curve (0.98 for this patient) and the mean of the upper Gaussian curve (2.07), respectively. By applying these thresholds within the target volume, we could then identify: hypoperfused voxels (hP_g , dark blue) and hyperperfused voxels (hP_g , red) (d). The site of relapse (light green) (f) was defined as any new contrast enhancement plus necrotic regions at relapse as compared to the nadir examination (after collapse of the surgical cavity) (e). Finally, the true positive voxels (yellow) were the site of relapse voxels within initial hP_g (f, g, h)

Delineation of anatomical regions of interest

For each patient, several anatomical regions of interest (ROIs) were manually delineated by one radiation oncologist (J.K.) with validation by a neuroradiologist (I.C.): contrast enhancement (CE) delineated on pre-RT T1-Gd, after subtraction of the surgical cavity, areas of hemorrhage defined on T1 WI pre-Gd and necrotic regions; hyperintensity on pre-RT FLAIR images (hyperFLAIR) excluding the surgical cavity, CE and necrotic regions; target volume (TV), defined as a 17-mm isotropic margin around the GTV with inclusion of all the FLAIR abnormalities; and site of relapse (SR), defined as CE plus necrotic regions at relapse, excluding CE plus necrotic regions or resection cavity before radiotherapy, or at nadir examination in the case of previous tumor shrinkage. The whole brain (WB) was also subjected to automatic segmentation and manual corrections.

Registration, data processing and volume analysis were performed with Sisyphé, an in-house neuro-imaging software toolbox [19].

rCBV and ADC maps

CBV maps were generated from DSC-MRI, as described previously [12], using dedicated FDA approved software (Olea Sphere®, V2.3, Olea Medical, La Ciotat, France), with an oscillation-index block-circulant singular value decomposition (oSVD) routine and correction for T1-weighted leakage effects. The CBV values of each patient were then normalized to the normal contralateral white-matter regions (as large as possible) in order to obtain relative CBV maps.

Using DWI data, ADC maps were also calculated on a voxel-by-voxel basis with the software incorporated into the MRI unit.

rCBV and ADC maps thresholding methods

Given that most relapses occur within the target volume (TV), all thresholding methods were applied within this volume.

We studied two rCBV map thresholding methods. The first was a fixed threshold method (t) based on a commonly used high rCBV threshold of 1.75 [11]. This threshold

was applied within the TV to extract the high rCBV voxels (hyperperfused voxels with fixed threshold: HP_t). The second was a Gaussian method (g) which utilized the normalized histogram plots of the total distribution of rCBV values within the TV. Since rCBV histograms were globally bimodal or skewed, a double Gaussian mixed model was used to provide optimal fitting. For each patient, we then defined the mean of the lower Gaussian curve and the mean of the upper one as hypoperfusion and hyperperfusion thresholds, respectively. Applying these thresholds, we then obtained: hyperperfused voxels with Gaussian method (HP_g), mid rCBV voxels, and hypoperfused voxels (hP_g) [20, 21]. This method was applied after excluding voxels with an rCBV <0.2, which might represent the surgical cavity or necrosis [12].

For the ADC map thresholding, owing to the absence of a commonly used fixed threshold, we only applied the Gaussian method to define: high ADC voxels, mid ADC voxels and low ADC voxels (diffusion-restricted voxels: DR_g).

We then defined several areas with perfusion and/or diffusion abnormalities (PDAs): HP_t , hP_g , HP_g , and DR_g . The value of HP_t and DR_g for predicting sites of relapse was assessed on a total of 2,459,483 voxels. The value of hP_g and HP_g was assessed on a total of 2,073,880 voxels.

Spatial analyses

Spatial analyses were performed using native resolution of the pre-RT T1-Gd MRI.

First, for each patient we analyzed the spatial distribution of PDA voxels within anatomical ROIs (CE, hyper-FLAIR, and TV) before radiotherapy.

Furthermore, we calculated the positive and negative predictive values (PPV/NPV) of PDAs within anatomical ROIs (hyperFLAIR or TV) as markers of subsequent sites of relapse after chemoradiation. Owing to the definition of the site of relapse (excluding pre-radiotherapy contrast enhancement), the CE ROI could not be analyzed to extract predictive values.

For the analysis, each voxel for each patient was classified as follows:

- true positive voxel (TPV): site of relapse (SR) voxel *within* ROI with initial PDA;
- false positive voxel (FPV): whole-brain (WB) voxel *outside* SR and *within* ROI with initial PDA;
- false negative voxel (FNV): SR voxel *within* ROI with no initial PDA;
- true negative voxel (TNV): WB voxel *outside* SR and *within* ROI with no initial PDA.

We then summed the TPVs, FNVs, FNVs and TNVs of all the patients to obtain the total numbers (Σ) of TPVs, FNVs, FNVs and TNVs within our population.

For each PDA, we therefore defined PPV and NPV for the pooled voxels as follows:

- $PPV = \Sigma TPVs / (\Sigma TPVs + \Sigma FNVs)$
- $NPV = \Sigma TNVs / (\Sigma TNVs + \Sigma FNVs)$.

The same method was applied for each patient to calculate PPV and NPV in a patient-by-patient basis.

Statistical analysis

PDA volumes were described in terms of median, range and standard deviation, and the spatial distribution of PDAs in terms of median and range.

The comparison of voxels characteristics was performed using the Chi square test. A Bonferroni correction was performed for multiple comparisons.

For all statistical tests, the significance level was set at 5%. Statistical analyses were performed using STATA 13.0 software (StataCorp LP, College Station, TX).

Results

Description of pre-radiotherapy PDAs volumes

Perfusion

Applying the 1.75 rCBV fixed threshold method, the median volume of HP_t was 19260 mm^3 ($8505\text{--}52638 \text{ mm}^3$).

Applying the Gaussian method, the median hypoperfusion threshold was 0.99 ± 0.26 and the median hyperperfusion threshold was 1.92 ± 0.32 . The median volume of hP_g was $21,093 \text{ mm}^3$ ($785\text{--}56830 \text{ mm}^3$), whereas the median volume of HP_g was $22,934 \text{ mm}^3$ ($5963\text{--}69,819 \text{ mm}^3$).

Diffusion

Applying the Gaussian method, the median low ADC threshold was $(808.5 \pm 105.5) \times 10^{-6} \text{ mm}^2/\text{s}$, and the median high ADC threshold was $(1097 \pm 234.9) \times 10^{-6} \text{ mm}^2/\text{s}$. The median volume of DR_g was $24,615 \text{ mm}^3$ ($13,257\text{--}48,728 \text{ mm}^3$).

Perfusion and diffusion

As HP_g was found to have the best PPV for site of relapse (cf Results), we decided to focus on the intersection between HP_g voxels and DR_g voxels ($HP_g \& DR_g$) (Fig. 3). The median volume of $HP_g \& DR_g$ was 2397.5 mm^3 ($769\text{--}20118 \text{ mm}^3$).

Spatial distribution of initial PDAs

The spatial distribution of PDAs within anatomical ROIs is summed up in Fig. 4.

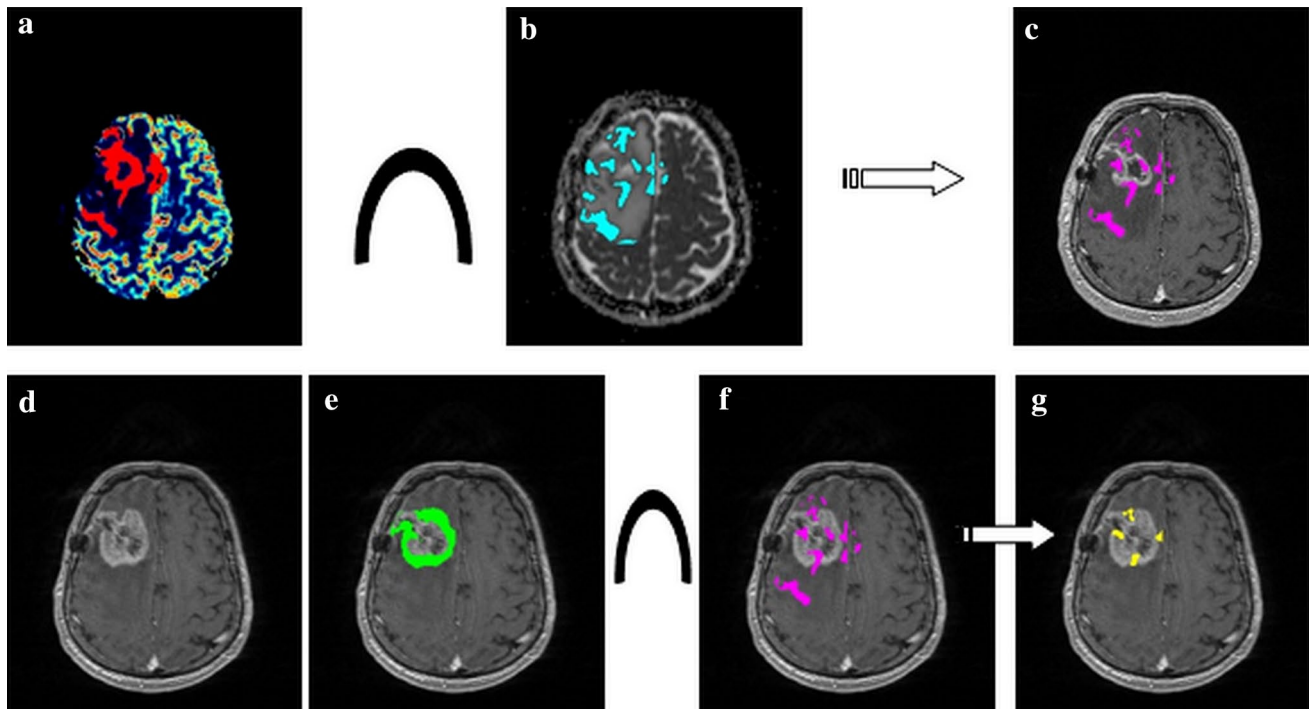


Fig. 3 Example of post-data processing to obtain HP_g & DR_g voxels. The Gaussian method was used to obtain hyperperfused voxels HP_g in red (a) and restricted-diffusion voxels DR_g in blue (b). The intersection between HP_g voxels and DR_g voxels allowed us to obtain HP_g & DR_g voxels in purple on the pre-RT T1-weighted images with gadolinium

(c). The MR scan at the time of relapse (d) was used to delineate the site of relapse in green as defined in our protocol (e). The true positive voxels in yellow (g) were the site of relapse voxels (e) within initial HP_g & DR_g voxels (f)

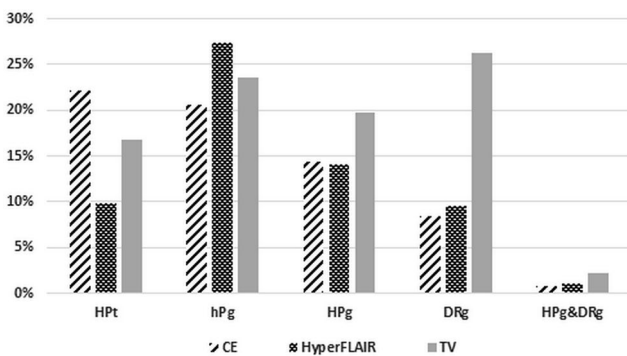


Fig. 4 Percentage of ROI volumes (CE, hyperFLAIR, TV) containing initial perfusion and/or diffusion abnormalities. The anatomical ROI volumes contained approximately 10–30% of initial PDAs, except for HP_g & DR_g voxels, which represented <5% of ROI volumes. PDA perfusion/diffusion abnormalities, HP_t hyperperfused voxels with fixed threshold method, hP_g hypoperfused voxels with Gaussian method, HP_g hyperperfused voxels with Gaussian method, HP_g & DR_g hyperperfused & diffusion-restricted voxels with Gaussian method, CE contrast enhancement, TV target volume

Predictive values for sites of relapse

The predictive values for sites of relapse according to the pooled-voxels quantification for the whole population, and by surgical status subgroup, are summarized in Table 2.

The best results were found using HP_g voxels: the PPV and NPV for sites of relapse within hyperFLAIR were 22.8 and 82.7%, respectively (Fig. 5).

We therefore decided to study the value of HP_g voxels with diffusion restriction (HP_g & DR_g voxels). In this case, 18.3% of hyperFLAIR voxels without initial PDAs were within sites of relapse versus 31.9% with initial PDAs ($p < 0.0001$) (Fig. 6).

The predictive values were also presented in a patient-by-patient basis in Table 3.

Discussion

Our results suggest that with the MRI protocols and image post-processing methods used in this study, neither DSC-MRI nor DWI is able to predict the sites of GBM relapse after chemoradiotherapy, even when these modalities are combined. The best results were obtained with HP_g & DR_g voxels within the hyperFLAIR volume (PPV of 31.9%). In other words, voxels with initial PDAs that were within hyperFLAIR or within the whole TV had a roughly 50% or a less than 50% probability of predicting the location of relapse, whatever the method of quantification (pooled-voxels or patient-by-patient analysis).

Table 2 Positive and negative predictive values for sites of relapse of perfusion/diffusion abnormalities voxels within hyperFLAIR and target volume ROIs, with a pooled-voxels quantification (for the whole cohort and according to the extent of resection, in *italics*)

PDA voxels	PPV (%)		NPV (%)	
	HyperFLAIR	TV	HyperFLAIR	TV
HP_t				
Whole cohort	21.6	9.5	82.4	88.3
<i>GTR subgroup</i>	<i>15.4</i>	<i>4.9</i>	<i>84.6</i>	<i>90.9</i>
<i>STR subgroup</i>	<i>24.8</i>	<i>14.2</i>	<i>81.5</i>	<i>86.3</i>
hP_g				
Whole cohort	13.8	10.9	80.5	87.1
<i>GTR subgroup</i>	<i>19.9</i>	<i>10.5</i>	<i>86</i>	<i>90.9</i>
<i>STR subgroup</i>	<i>11.3</i>	<i>11.4</i>	<i>78.1</i>	<i>84.7</i>
HP_g				
Whole cohort	22.8	12.9	82.7	87.7
<i>GTR subgroup</i>	<i>14.3</i>	<i>8.8</i>	<i>84.4</i>	<i>90.4</i>
<i>STR subgroup</i>	<i>26.8</i>	<i>15.1</i>	<i>82</i>	<i>85.6</i>
DR_g				
Whole cohort	16.9	10.8	81.6	87.8
<i>GTR subgroup</i>	<i>25.1</i>	<i>8.6</i>	<i>83.6</i>	<i>90.6</i>
<i>STR subgroup</i>	<i>13.9</i>	<i>12.4</i>	<i>80.9</i>	<i>86</i>
HP_g&DR_g				
Whole cohort	31.9	18.5	81.7	88
<i>GTR subgroup</i>	<i>48.1</i>	<i>15.1</i>	<i>83.3</i>	<i>90.3</i>
<i>STR subgroup</i>	<i>25.4</i>	<i>19.9</i>	<i>81.1</i>	<i>86.6</i>

PDA perfusion/diffusion abnormalities, PPV positive predictive value, NPV negative predictive value, TV target volume, HP_t hyperperfused voxels with fixed threshold method, hP_g hypoperfused voxels with Gaussian method, HP_g hyperperfused voxels with Gaussian method, HP_g&DR_g hyperperfused & diffusion restricted voxels with Gaussian method, GTR gross total resection subgroup, STR subtotal resection subgroup

Our study seems robust in terms of both material and method. Indeed, a major strength of this study is its prospective design, with the same MR acquisition parameters, the same treatment modalities and follow-up for every patient from each centre. Each patient received the current standard of care with chemoradiation [1], allowing us to easily extrapolate our results. The gold-standard to define relapse is a tissue based analysis; however, it only provides a small sample of a region of interest, rather than a precise cartography of the status of each voxel. Instead, relapse was defined according to the well-established RANO criteria. Admittedly, contrast enhancement is not the full histopathological extent of recurrent tumor. However, this approach could be explained by the difficulty to differentiate between non-tumoral vasogenic-edema versus tumor-infiltrative area within the non-enhancing FLAIR hyperintensity lesion in T2-weighted sequences. Only a few studies have attempted to classify the non-enhancing lesion area in order to identify infiltrative tumor area, using conventional imaging or

advanced imaging methods, but with uncertain efficacy [32–35]. None of these methods has been clearly validated, and therefore T2-weighted images do not seem to localize an area of recurrence with precision, contrary to an increase of or an apparition of contrast enhancement. The inclusion of the hypersignal FLAIR in the site of relapse would have then introduced a high degree of uncertainty in our approach.

The use of post-surgical images as baseline prevented from huge local changes after surgery, although postsurgical changes (resolution of edema, tumor shrinkage...) cannot be ignored. However, these post-surgical changes have been taken into account in some extent for the definition of the site of relapse, as illustrated in Figs. 1 and 2. Indeed, the site of relapse was defined optimally by using the nadir of the lesion for each patient, in order to take into account any tumor shrinkage or cavity collapse during the follow-up.

We decided to enroll both STR and GTR patients to increase the statistical power because we hypothesized that the predictive value of PDAs within hyperFLAIR (the first ROI) to predict recurrence was not affected by the extent of resection, as any residual enhancing tumor has been excluded from hyperFLAIR. Regarding the TV ROI (including the residual contrast enhancing region), our results showed that the predictive values in the STR group were slightly and inconstantly better than in the GTR group, and still low, suggesting that the extent of surgical resection is not a real caveat in our analysis even after consideration of the residual contrast enhancing region. However, we admit that our small series of patients is also heterogeneous in terms of age and MGMT methylation status, which precludes any subgroup analysis to assess the value of perfusion or diffusion MRI to predict the sites of relapse.

Lastly, despite the relatively small sample size of patients of our pilot study, the pooled-voxels quantification approach with large sets of voxels ensured a robust statistical power. Although we should bear in mind that some degree of spatial correlation exists in imaging data between neighbouring voxels, an alternative approach using “resels” (a block of voxels regarded as independent elements [22]) instead of voxels would not have really impacted our results, as the predictive values were a ratio between two amounts of voxels.

Regarding technical considerations, one possible limitation is the rigid-body co-registration that was employed. However, since we did not use a parametric response map [23–26] but instead a voxel-based quantification of an overlap, a misregistration of a few millimetres would have led to uncertainties at the edge of the overlap only, but not in the core of the overlap. Moreover, even voxel-wise parametric response map studies only assessed rigid-body coregistrations, demonstrating the continuing need for caution in the integration of non-linear co-registrations [23–26].

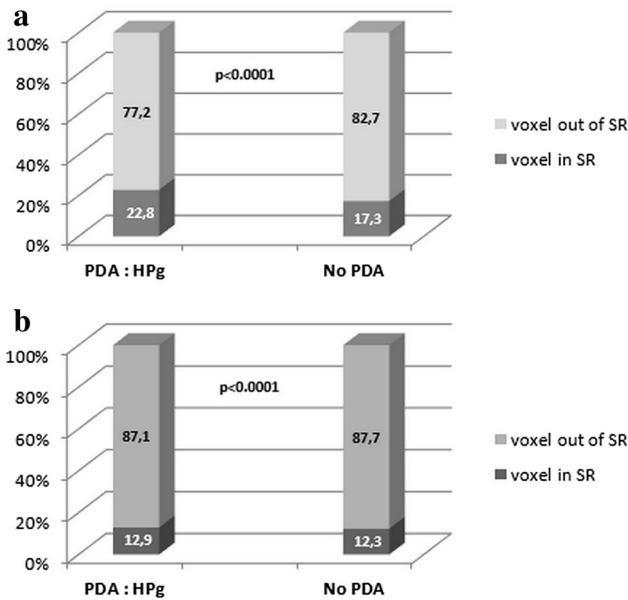


Fig. 5 Evaluation of hyperperfused voxels HP_g defined with the Gaussian method as a predictive marker of sites of relapse after chemoradiation, (a) within hyperFLAIR, (b) within target volume. *SR* sites of relapse, *PDA* perfusion/diffusion abnormalities

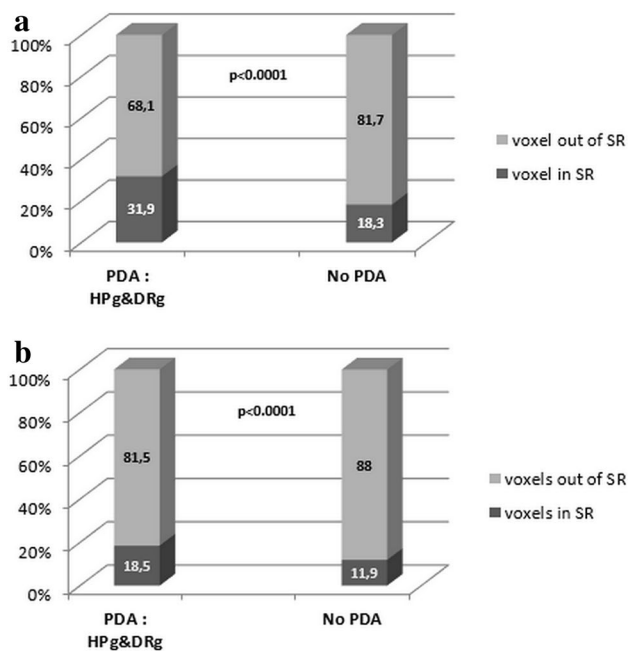


Fig. 6 Evaluation of hyperperfused and diffusion restriction voxels $HP_g \& DR_g$ defined with the Gaussian method as a predictive marker of sites of relapse after chemoradiation, (a) within hyperFLAIR, (b) within target volume. *SR* sites of relapse, *PDA* perfusion/diffusion abnormalities

Two major technical strengths of our method also deserve to be highlighted. First, our post-processing method using oSVD deconvolution was delay-insensitive [27] and allowed for a more robust and accurate estimation of CBV

[28]. Moreover, it used leakage correction using K2 maps in order to maximize CBV accuracy in neovascular lesions [29–31]. The second strength concerned the use of more than one thresholding method in order to avoid a thresholding bias. The first method was based on a commonly used rCBV fixed hyperperfusion threshold of 1.75 [11]. We did not find such a robust ADC threshold in previous studies. The second method using a Gaussian approach allowed us to isolate hypoperfusion/hyperperfusion and restricted diffusion voxels without any pre-defined thresholds [20].

Many studies have already established the value of rCBV or ADC to predict the histopathological grade of tumors [11, 32, 33] or the overall and progression-free survival rates at diagnosis [11, 34–36], and as early surrogate markers for treatment response: either in a global approach [12, 37, 38], or more recently in a voxel-wise approach to define a parametric response map [23, 24, 26, 39]. By contrast, to our knowledge, this study is the first study with a pooled voxels quantification to have assessed the predictive value of pre-radiotherapy DSC-MRI and/or DWI to locate sites of relapse after chemoradiation for GBM. The value of pre-RT ADC for predicting the location of relapse has been assessed in a single recent study, which reported that restricted diffusion overlapped with the recurrence in 28/32 patients (88%), with a mean hypointensity overlap ratio of 60% [16]. However, this retrospective study contained several limitations. The overlap ratio was only calculated with a patient-by-patient approach, and not with a pooled-voxels analysis, so the volume of recurrence should have been weighted. The delineation of ADC hypointensity was manually performed, without a reproducible threshold. Furthermore, the delineation of the relapse was not accurately described. Similarly for rCBV, a small retrospective non-voxel-wise study also found that areas with a future focal recurrence within a 2-cm margin after gross total resection retrospectively had a trend toward higher median rCBV than other areas on immediate post-operative MRI. However, as no attempt was made to prospectively identify and validate high-risk rCBV voxels or areas, no predictive data of perfusion abnormality could be extracted, as was performed in our study [40]. Lastly, the value of voxels combining both perfusion and diffusion abnormalities to predict sites of relapse had never been explored before.

With the increasing inclusion of metabolic imaging within radiotherapy treatment planning systems [41] in order to target contrast enhanced or metabolic abnormalities, *dose-painting* approaches based on a multi-target strategy are bringing new hope for better tumor control in GBM [42, 43]. Several radioresistant targets have already been identified which could be predictive of relapse. Indeed, several studies have shown that spectral abnormalities (choline/NAA >2 or lactate/NAA >0.4) are predictive of the sites of relapse [6–9], and have given rise to an ongoing French

Table 3 Median positive and negative predictive values for sites of relapse of perfusion/diffusion abnormalities voxels within hyper-FLAIR and target volume ROIs, with a patient-by-patient analysis (for the whole cohort and according to the extent of resection, in *italics*)

PDA voxels	PPV (%)		NPV (%)	
	HyperFLAIR	TV	HyperFLAIR	TV
HP_t				
Whole cohort	24.8	9.3	80.3	91
<i>GTR subgroup</i>	<i>23</i>	<i>5.8</i>	<i>80.9</i>	<i>95.8</i>
<i>STR subgroup</i>	<i>31.3</i>	<i>13.2</i>	<i>80.3</i>	<i>90.8</i>
hP_g				
Whole cohort	16.8	7.2	78.6	90.8
<i>GTR subgroup</i>	<i>21.1</i>	<i>3.4</i>	<i>79.8</i>	<i>94.5</i>
<i>STR subgroup</i>	<i>16.8</i>	<i>8.0</i>	<i>78.6</i>	<i>86.9</i>
HP_g				
Whole cohort	28.8	13.5	81.2	89.9
<i>GTR subgroup</i>	<i>26.2</i>	<i>8.2</i>	<i>80.9</i>	<i>95.6</i>
<i>STR subgroup</i>	<i>32.8</i>	<i>14.2</i>	<i>81.2</i>	<i>89.3</i>
DR_g				
Whole cohort	28.5	8.9	79.4	91.1
<i>GTR subgroup</i>	<i>31.4</i>	<i>6.2</i>	<i>78.5</i>	<i>95.2</i>
<i>STR subgroup</i>	<i>16.8</i>	<i>9.3</i>	<i>80.3</i>	<i>90.5</i>
HP_g&DR_g				
Whole cohort	52.1	24.3	78.7	91.7
<i>GTR subgroup</i>	<i>50.6</i>	<i>26.2</i>	<i>77.5</i>	<i>96.3</i>
<i>STR subgroup</i>	<i>53.7</i>	<i>22.3</i>	<i>79.9</i>	<i>91.1</i>

PDA perfusion/diffusion abnormalities, PPV positive predictive value, NPV negative predictive value, TV target volume, HP_t hyperperfused voxels with fixed threshold method, hP_g hypoperfused voxels with Gaussian method, HP_g hyperperfused voxels with Gaussian method, HP_g&DR_g hyperperfused & diffusion restricted voxels with Gaussian method, GTR gross total resection subgroup, STR subtotal resection subgroup

multicentre randomized trial assessing the benefit of dose escalation on spectral abnormalities in a *dose-painting* approach (NCT01507506). A similar prospective trial is also about to start in the United States [44] (NCT02394665). Regarding positron emission tomography (PET), a recent approach has been developed which uses 11C-methionine (MET-PET), as high-uptake volumes were found to be associated with areas at risk of relapse [45], leading to a prospective trial to confirm these correlations (NCT01873469), before developing a *dose-painting* approach.

Regarding perfusion and diffusion MRI data, they are broadly considered to be correlated to GBM histopathologic features of aggressiveness. For example, Barajas et al. have observed a positive correlation between rCBV and microvascular expression, hypoxia, cellular mitosis, and overall cellularity in GBM, and an inverse correlation between ADC and the same histopathologic features [46]. However, similar studies have yielded mixed findings with weaker correlations with both rCBV and ADC [47–51]. Indeed, a

partial mismatch between microvessel density or angiogenesis and blood volume determinations could be explained by the fact that the tumor vessels, which are mainly made up of non functional immature capillaries with a narrow lumen with no blood flow [52], will not contribute to the rCBV. Likewise, many factors have been described to influence the degree to which water molecular motion is reduced within gliomas, including nuclear-to-cytoplasmic ratio, cellular density, necrosis, intra- and extra-cellular edema and extra-cellular matrix components [47–49, 51, 53]. These complex interactions of water diffusivity within the heterogeneous inter and intracellular environment of gliomas can thus yield unpredictable ADC values within a voxel. As mentioned earlier, rCBV and ADC are both described as being predictive of outcome, because they seem to be *globally* correlated to histopathologic features. However, the weakness of the correlation in some parts of the tumor and the complexity of processes at a tissue level such as neoangiogenesis or cell proliferation within a single voxel do not enable to establish an accurate cartography of high risk of relapse areas using only rCBV and ADC. Besides, rCBV and ADC do not assess the metabolism of the tumor, as MRI spectroscopy and MET-PET do. Imaging that does predict the sites of relapse after chemoradiotherapy may reflect areas of radio-resistant cells that are usually linked to a specific tumor-cell metabolism, such as acidosis, whereas DSC-MRI or DWI seem more reflective of a histopathologic feature. All these reasons could be advanced to explain why rCBV and ADC do not seem to help in predicting which areas are at risk of relapse after chemoradiotherapy. However, although the other parameters extracted from DSC are less frequently used in clinical routine compared to rCBV, further analyses should be performed in the same way with relative cerebral blood flow, median time of transit or time to peak.

In conclusion, our results based on a large set of voxels in a prospective trial suggest that DSC and DWI-MRI do not predict the GBM relapse sites. Based upon these preliminary results, at this stage, we cannot support the use of these techniques to guide focal increases in radiotherapy doses. However, further investigations with new methodological approaches and extended cohorts are needed in order to better understand the role of these modalities in the prediction of glioblastoma relapse sites, and to optimally integrate them in the radiotherapy treatment planning process.

Acknowledgments The authors would like to thank Soléakhena Ken and Amandine Fabre for assistance to collect imaging data.

Funding None.

Compliance with ethical standards

Conflict of interest The authors declare that they have no conflict of interest.

References

- Stupp R, Mason WP, van den Bent MJ et al (2005) Radiotherapy plus concomitant and adjuvant temozolomide for glioblastoma. *N Engl J Med* 352:987–996
- Kantor G, Loiseau H (2005) Analysis of target volumes for gliomas. *Cancer Radiother* 9:230–239
- Chang EL, Akyurek S, Avalos T et al (2007) Evaluation of peritumoral edema in the delineation of radiotherapy clinical target volumes for glioblastoma. *Int J Radiat Oncol Biol Phys* 68:144–150
- Minniti G, Amelio D, Amichetti M, Salvati M, Muni R, Bozzao A, Lanzetta G, Scarpino S, Arcella A, Enrici RM (2010) Patterns of failure and comparison of different target volume delineations in patients with glioblastoma treated with conformal radiotherapy plus concomitant and adjuvant temozolomide. *Radiother Oncol* 97:377–381
- Ling CC, Humm J, Larson S, Amols H, Fuks Z, Leibel S, Koutcher JA (2000) Towards multidimensional radiotherapy (MD-CRT): biological imaging and biological conformality. *Int J Radiat Oncol Biol Phys* 47:551–560
- Pirzkall A, Li X, Oh J, Chang S, Berger MS, Larson DA, Verhey LJ, Dillon WP, Nelson SJ (2004) 3D MRSI for resected high-grade gliomas before RT: tumor extent according to metabolic activity in relation to MRI. *Int J Radiat Oncol Biol Phys* 59:126–137
- Park I, Tamai G, Lee MC, Chuang CF, Chang SM, Berger MS, Nelson SJ, Pirzkall A (2007) Patterns of recurrence analysis in newly diagnosed glioblastoma multiforme after three-dimensional conformal radiation therapy with respect to pre-radiation therapy magnetic resonance spectroscopic findings. *Int J Radiat Oncol Biol Phys* 69:381–389
- Laprie A, Catalaa I, Cassol E, McKnight TR, Berchery D, Marre D, Bachaud J-M, Berry I, Moyal EC-J (2008) Proton magnetic resonance spectroscopic imaging in newly diagnosed glioblastoma: predictive value for the site of postradiotherapy relapse in a prospective longitudinal study. *Int J Radiat Oncol Biol Phys* 70:773–781
- Deviars A, Ken S, Filleron T et al (2014) Evaluation of the lactate-to-*N*-acetyl-aspartate ratio defined with magnetic resonance spectroscopic imaging before radiation therapy as a new predictive marker of the site of relapse in patients with glioblastoma multiforme. *Int J Radiat Oncol Biol Phys* 90:385–393
- Cao Y, Sundgren PC, Tsien CI, Chenevert TT, Junck L (2006) Physiologic and metabolic magnetic resonance imaging in gliomas. *J Clin Oncol* 24:1228–1235
- Law M, Young RJ, Babb JS, Peccerelli N, Chheang S, Gruber ML, Miller DC, Golfinos JG, Zagzag D, Johnson G (2008) Gliomas: predicting time to progression or survival with cerebral blood volume measurements at dynamic susceptibility-weighted contrast-enhanced perfusion MR imaging. *Radiology* 247:490–498
- Cao Y, Tsien CI, Nagesh V, Junck L, Ten Haken R, Ross BD, Chenevert TL, Lawrence TS (2006) Survival prediction in high-grade gliomas by MRI perfusion before and during early stage of RT [corrected]. *Int J Radiat Oncol Biol Phys* 64:876–885
- Tsien C, Cao Y, Chenevert T (2014) Clinical applications for diffusion magnetic resonance imaging in radiotherapy. *Semin Radiat Oncol* 24:218–226
- Catalaa I, Henry R, Dillon WP, Graves EE, McKnight TR, Lu Y, Vigneron DB, Nelson SJ (2006) Perfusion, diffusion and spectroscopy values in newly diagnosed cerebral gliomas. *NMR Biomed* 19:463–475
- Deike K, Wiestler B, Graf M et al (2015) Prognostic value of combined visualization of MR diffusion and perfusion maps in glioblastoma. *J Neurooncol*. doi:10.1007/s11060-015-1982-z
- Elson A, Paulson E, Bovi J, Siker M, Schultz C, Lavolette PS (2015) Evaluation of pre-radiotherapy apparent diffusion coefficient (ADC): patterns of recurrence and survival outcomes analysis in patients treated for glioblastoma multiforme. *J Neurooncol*. doi:10.1007/s11060-015-1782-5
- Wen PY, Macdonald DR, Reardon DA et al (2010) Updated response assessment criteria for high-grade gliomas: response assessment in neuro-oncology working group. *J Clin Oncol* 28:1963–1972
- Meyer CR, Boes JL, Kim B, Bland PH, Zasadny KR, Kison P V, Koral K, Frey KA, Wahl RL (1997) Demonstration of accuracy and clinical versatility of mutual information for automatic multimodality image fusion using affine and thin-plate spline warped geometric deformations. *Med Image Anal* 1:195–206
- Tensaouti F, Lotterie JA, Clarisse P et al (2008) Sisyphus-neuroimaging software toolbox. In: Proceedings of ESMRMB Congress, Valencia, Spain (abstract 991)
- Pope WB, Kim HJ, Huo J et al (2009) Recurrent glioblastoma multiforme: ADC histogram analysis predicts response to bevacizumab treatment. *Radiology* 252:182–189
- Ellingson BM, Sahebjam S, Kim HJ, Pope WB, Harris RJ, Woodworth DC, Lai A, Nghiemphu PL, Mason WP, Cloughesy TF (2014) Pretreatment ADC histogram analysis is a predictive imaging biomarker for bevacizumab treatment but not chemotherapy in recurrent glioblastoma. *AJNR Am J Neuroradiol* 35:673–679
- Worsley KJ, Evans AC, Marrett S, Neelin P (1992) A three-dimensional statistical analysis for CBF activation studies in human brain. *J Cereb Blood Flow Metab* 12:900–918
- Moffat BA, Chenevert TL, Lawrence TS et al (2005) Functional diffusion map: a noninvasive MRI biomarker for early stratification of clinical brain tumor response. *Proc Natl Acad Sci USA* 102:5524–5529
- Galbán CJ, Chenevert TL, Meyer CR et al (2009) The parametric response map is an imaging biomarker for early cancer treatment outcome. *Nat Med* 15:572–576
- Tsien C, Galbán CJ, Chenevert TL et al (2010) Parametric response map as an imaging biomarker to distinguish progression from pseudoprogression in high-grade glioma. *J Clin Oncol* 28:2293–2299
- Lemasson B, Chenevert TL, Lawrence TS et al (2013) Impact of perfusion map analysis on early survival prediction accuracy in glioma patients. *Transl. Oncol* 6:766–774
- Ostergaard L, Weisskoff RM, Chesler DA, Gyldensted C, Rosen BR (1996) High resolution measurement of cerebral blood flow using intravascular tracer bolus passages. Part I: mathematical approach and statistical analysis. *Magn Reson Med* 36:715–725
- Wu O, Østergaard L, Weisskoff RM, Benner T, Rosen BR, Sorensen AG (2003) Tracer arrival timing-insensitive technique for estimating flow in MR perfusion-weighted imaging using singular value decomposition with a block-circulant deconvolution matrix. *Magn Reson Med* 50:164–174
- Hu LS, Baxter LC, Pinnaduwege DS et al (2010) Optimized preload leakage-correction methods to improve the diagnostic accuracy of dynamic susceptibility-weighted contrast-enhanced perfusion MR imaging in posttreatment gliomas. *AJNR Am J Neuroradiol* 31:40–48
- Law M, Yang S, Babb JS, Knopp EA, Golfinos JG, Zagzag D, Johnson G (2004) Comparison of cerebral blood volume and vascular permeability from dynamic susceptibility contrast-enhanced perfusion MR imaging with glioma grade. *AJNR Am J Neuroradiol* 25:746–755
- Paulson ES, Schmainda KM (2008) Comparison of dynamic susceptibility-weighted contrast-enhanced MR methods: recommendations for measuring relative cerebral blood volume in brain tumors. *Radiology* 249:601–613

32. Law M, Yang S, Wang H, Babb JS, Johnson G, Cha S, Knopp EA, Zagzag D (2003) Glioma grading: sensitivity, specificity, and predictive values of perfusion MR imaging and proton MR spectroscopic imaging compared with conventional MR imaging. *AJNR Am J Neuroradiol* 24:1989–1998
33. Sadeghi N, Salmon I, Decaestecker C et al (2007) Stereotactic comparison among cerebral blood volume, methionine uptake, and histopathology in brain glioma. *AJNR Am J Neuroradiol* 28:455–461
34. Lev MH, Ozsunar Y, Henson JW et al (2004) Glial tumor grading and outcome prediction using dynamic spin-echo MR susceptibility mapping compared with conventional contrast-enhanced MR: confounding effect of elevated rCBV of oligodendrogliomas [corrected]. *AJNR Am J Neuroradiol* 25:214–221
35. Murakami R, Sugahara T, Nakamura H, Hirai T, Kitajima M, Hayashida Y, Baba Y, Oya N, Kuratsu J-I, Yamashita Y (2007) Malignant supratentorial astrocytoma treated with postoperative radiation therapy: prognostic value of pretreatment quantitative diffusion-weighted MR imaging. *Radiology* 243:493–499
36. Yamasaki F, Sugiyama K, Ohtaki M et al (2010) Glioblastoma treated with postoperative radio-chemotherapy: prognostic value of apparent diffusion coefficient at MR imaging. *Eur J Radiol* 73:532–537
37. Kim JH, Choi SH, Ryoo I et al (2014) Prognosis prediction of measurable enhancing lesion after completion of standard concomitant chemoradiotherapy and adjuvant temozolomide in glioblastoma patients: application of dynamic susceptibility contrast perfusion and diffusion-weighted imaging. *PLoS One* 9:e113587
38. Mardor Y, Pfeffer R, Spiegelmann R et al (2003) Early detection of response to radiation therapy in patients with brain malignancies using conventional and high b-value diffusion-weighted magnetic resonance imaging. *J Clin Oncol* 21:1094–1100
39. Hamstra DA, Galbán CJ, Meyer CR et al (2008) Functional diffusion map as an early imaging biomarker for high-grade glioma: correlation with conventional radiologic response and overall survival. *J Clin Oncol* 26:3387–3394
40. Smets T, Lawson TM, Grandin C, Jankovski A, Raftopoulos C (2013) Immediate post-operative MRI suggestive of the site and timing of glioblastoma recurrence after gross total resection: a retrospective longitudinal preliminary study. *Eur Radiol* 23:1467–1477
41. Ken S, Vieilleveigne L, Franceries X et al (2013) Integration method of 3D MR spectroscopy into treatment planning system for glioblastoma IMRT dose painting with integrated simultaneous boost. *Radiat Oncol* 8:1
42. Piroth MD, Pinkawa M, Holy R et al (2012) Integrated boost IMRT with FET-PET-adapted local dose escalation in glioblastomas. Results of a prospective phase II study. *Strahlenther Onkol* 188:334–339
43. Tsien CI, Brown D, Normolle D et al (2012) Concurrent temozolomide and dose-escalated intensity-modulated radiation therapy in newly diagnosed glioblastoma. *Clin Cancer Res* 18:273–279
44. Parra NA, Maudsley AA, Gupta RK et al (2014) Volumetric spectroscopic imaging of glioblastoma multiforme radiation treatment volumes. *Int J Radiat Oncol Biol Phys* 90:376–384
45. Lee IH, Piert M, Gomez-Hassan D, Junck L, Rogers L, Hayman J, Ten Haken RK, Lawrence TS, Cao Y, Tsien C (2009) Association of 11C-methionine PET uptake with site of failure after concurrent temozolomide and radiation for primary glioblastoma multiforme. *Int J Radiat Oncol Biol Phys* 73:479–485
46. Barajas RF, Hodgson JG, Chang JS, Vandenberg SR, Yeh R-F, Parsa AT, McDermott MW, Berger MS, Dillon WP, Cha S (2010) Glioblastoma multiforme regional genetic and cellular expression patterns: influence on anatomic and physiologic MR imaging. *Radiology* 254:564–576
47. Guo AC, Cummings TJ, Dash RC, Provenzale JM (2002) Lymphomas and high-grade astrocytomas: comparison of water diffusibility and histologic characteristics. *Radiology* 224:177–183
48. Sugahara T, Korogi Y, Kochi M et al (1999) Usefulness of diffusion-weighted MRI with echo-planar technique in the evaluation of cellularity in gliomas. *J Magn Reson Imaging* 9:53–60
49. Gupta RK, Cloughesy TF, Sinha U, Garakian J, Lazareff J, Rubino G, Rubino L, Becker DP, Vinters HV, Alger JR (2000) Relationships between choline magnetic resonance spectroscopy, apparent diffusion coefficient and quantitative histopathology in human glioma. *J Neurooncol* 50:215–226
50. Sadeghi N, D’Haene N, Decaestecker C, Levivier M, Metens T, Maris C, Wikler D, Baleriaux D, Salmon I, Goldman S (2008) Apparent diffusion coefficient and cerebral blood volume in brain gliomas: relation to tumor cell density and tumor microvessel density based on stereotactic biopsies. *AJNR Am J Neuroradiol* 29:476–482
51. Stadnik TW, Chaskis C, Michotte A, Shabana WM, van Rompaey K, Luypaert R, Budinsky L, Jellus V, Osteaux M (2001) Diffusion-weighted MR imaging of intracerebral masses: comparison with conventional MR imaging and histologic findings. *AJNR Am J Neuroradiol* 22:969–976
52. Miyagami M, Katayama Y (2005) Angiogenesis of glioma: evaluation of ultrastructural characteristics of microvessels and tubular bodies (Weibel-Palade) in endothelial cells and immunohistochemical findings with VEGF and p53 protein. *Med Mol Morphol* 38:36–42
53. Sadeghi N, Camby I, Goldman S, Gabius H-J, Balériaux D, Salmon I, Decaestecker C, Kiss R, Metens T (2003) Effect of hydrophilic components of the extracellular matrix on quantifiable diffusion-weighted imaging of human gliomas: preliminary results of correlating apparent diffusion coefficient values and hyaluronan expression level. *AJR Am J Roentgenol* 181:235–241